Journal of Microbiology (2015) Vol. 53, No. 1, pp. 32–37
DOI 10.1007/s12275-015-4539-0

Crystal structure of the bacterial type VI secretion system component TssL from *Vibrio cholerae*

Jeong Ho Chang[1] and Yeon-Gil Kim[2*]

[1]*Department of Biology, Teachers College, Kyungpook National University, Daegu 702-701, Republic of Korea*
[2]*Beamline Science Division, Pohang Accelerator Laboratory, Pohang 790-784, Republic of Korea*

(Received Sep 26, 2014 / Revised Oct 27, 2014 / Accepted Oct 27, 2014)

The type VI secretion system (T6SS), commonly found in Gram-negative bacteria, is responsible for exporting effector proteins. The T6SS has been reported to be cytotoxic to host cells. While the components and assembly of the T6SS complex have been largely assessed, structural data on T6SS components from virulent bacteria is remarkably insufficient. Here, we report the crystal structure of *Vibrio cholerae* TssL (VcTssL), a core component of T6SS. In spite of a relatively low sequence identity, the overall structure of VcTssL is largely similar to those from other bacterial homologs except for several differences found in local structural elements. A unique feature attributed to the C-terminal fragment of VcTssL is a crystallographic artifact. This incidental feature of VcTssL may provide insights into screening of molecular partners for the cytoplasmic domain of TssL. Additionally, our results may help in the design of molecular probes for a detailed understanding of the functional relationship between TssL and other T6SS components.

Keywords: type VI secretion system, TssL, *Vibrio cholerae*, X-ray crystallography

Introduction

At least six types of secretion systems have been found in gram-negative bacteria that differ in their structural components and characteristic subcellular pathways during export events (Economou *et al.*, 2006). The complex of type VI secretion system (T6SS) is found in Gram-negative bacteria and is involved in the interaction between pathogenic bacteria and their hosts (Jani and Cotter, 2010; Schwarz *et al.*, 2010; Russell *et al.*, 2014). It has been previously reported that T6SS has cytotoxic effects and plays a role in inter-bacterial relationships, biofilm formation, and survival in phagocytic cells (Cascales, 2008; Pukatzki *et al.*, 2009; Miyata *et al.*, 2010). The cytotoxic effects are due to the T6SS-mediated translocation of effector molecules into the recipient host cells via a membrane-spanning tubular complex (Filloux, 2009; Russell *et al.*, 2011).

The T6SS complex consists of 13 conserved core components and several additional accessory subunits that form an injector like structure (Bingle *et al.*, 2008; Zoued *et al.*, 2014). Based on their proposed functions, the core components of T6SS can be divided into two categories: bacteriophage-like subunits and membrane-associated subunits (Silverman *et al.*, 2012). At least two bacteriophage related subunits Hcp (hemolysin-coregulated protein) and VgrG (valine-glycine repeat protein) were identified by infected eukaryotic cell culture supernatants (Cascales, 2008). To date, 7 more subunits have been identified and have been assigned the function of construction of the bacteriophage tail like structure because of their structural similarities (Zoued *et al.*, 2014). The membrane associated components are known to play key roles in formation of membrane complex, composed of four subunits TssL, TssM, TssJ, and TagL (Aschtgen *et al.*, 2010; Felisberto-Rodrigues *et al.*, 2011). The membrane complex is thought to be involved in the assembly of the T6SS over the bacterial cell envelope. While most subunits of the T6SSare identified, additional studies would be required to address the complete function of T6SS.

Vibrio cholerae is a Gram-negative bacterium and the causative agent of cholera, which is a severe diarrheal disease. Infection occurs mainly due to ingestion of contaminated food or water. The main symptom, excessive secretory diarrhea, results in over-dehydration and may also lead to death if it is not cured immediately (Faruque *et al.*, 1998). The virulence factor cholera toxin (CT) leads to diarrhea by correlatively regulating the expression of toxin co-regulated pili (TCP) responsible for colonization in the intestinal epithelium. Moreover, the T6SS is implicated as an additional virulence factor of *V. cholerae* based on studies using eukaryotic slime mold *Dictyostelium discoideum* and infant animal infection models such as mouse and rabbit (Ma and Mekalanos, 2010; Zheng *et al.*, 2010). Additionally, the *V. cholerae* T6SS shows antimicrobial properties and brings about a drastic reduction in *Escherichia coli* K2 survival when cultured together (MacIntyre *et al.*, 2010). The T6SS in *V. cholerae* also plays a role for in Hcp as well as three VgrG proteins (Pukatzki *et al.*, 2006).

Recent structural studies on T6SS have largely followed after functional investigations. In the T6SS molecular architecture, TssL is a core subunit and a membrane associated component. The C-terminal single transmembrane part of TssL is responsible for anchoring in the inner membrane of bacterial envelope as well as for association with TssM subunit (Aschtgen *et al.*, 2012; Cascales and Cambillau, 2012). Recently, two crystal structures of the cytoplasmic

*For correspondence. E-mail: ygkim76@postech.ac.kr; Tel.: +82-54-279-1544

domain of TssL viz. from *E. coli* (EcTssL) and *Francisella novicida* (FnTssL) have been reported (Durand *et al.*, 2012; Robb *et al.*, 2012). TssL from *V. cholerae* shares relatively low sequence identity (less than 20%) with either EcTssL or FnTssL. This suggests that the cellular function of TssL is largely dependent on its unique structural elements. Since structural information on T6SS components from this significant pathogen is sparse, the crystal structure of TssL from *V. cholerae* may provide insights into the functional mechanism of the T6SS apparatus.

Materials and Methods

Cloning, protein expression, and protein purification

The TssL gene (UniProt ID, Q9KN50) was amplified from *V. cholerae* genome by standard PCR and the PCR product was sequenced to confirm the absence of mutations. The amplified gene was inserted into the pET-30a vector (Invitrogen) using *Nde*I and *Xho*I restriction sites. The recombinant plasmid was transformed into *E. coli* BL21 (DE3) cells, which were grown at 37°C in LB medium containing 50 mg/ml kanamycin till an A_{600} of 0.8 was reached after which protein expression was induced with 0.5 mM isopropyl β-D-1-thiogalactopyranoside (IPTG) at 18°C for 12 h.

C-terminal 6X His-tagged proteins were purified as suggested. Briefly, induced cells were harvested by centrifugation at 5,000 × g at 4°C for 20 min and lysed by sonication in a buffer containing 30 mM Tris-HCl (pH 8.0), 300 mM NaCl. Debris were removed by centrifugation at 15,000 × *g* for 30 min and the supernatant was loaded onto Ni-NTA resin (Qiagen). After washing with 20 mM imidazole to remove unbound or nonspecifically bound protein, the bound protein was eluted in step gradient using 30 mM Tris-HCl (pH 8.0), 50 mM NaCl, 200 mM imidazole. The eluted protein was further purified using HiTrap Q (GE Healthcare) by a NaCl gradient (50–500 mM), and finally, by using a Superdex 75 26/60 prep-grade (GE Healthcare) column equilibrated with 10 mM Tris-HCl (pH 8.0), 100 mM NaCl. The purified protein was finally concentrated to 20 mg/ml. Aliquots were flash-frozen in liquid nitrogen and stored at -80°C.

Crystallization

In order to facilitate the crystallization of TssL, the purified protein was subjected to limited proteolysis with trypsin (Calbiochem). Trypsin was added in a 10000^{-1} ratio for TssL protein [~20 mg/ml in buffer containing of 10 mM Tris-HCl (pH 8.0), 100 mM NaCl, 10 mM $CaCl_2$] and digestion was carried out at 297 K for 4 h and was stopped by the addition of 1 mM phenylmethylsulfonyl fluoride (PMSF, Sigma). The digested sample was used directly for crystallization without further purification. Crystallization was carried out by the sitting-drop vapour-diffusion method in 96-well sitting-drop crystallization plates (Axygen). All crystallization trials were carried out at 22°C. Initial crystals were obtained in the condition containing 2.5 M sodium chloride, 100 mM sodium potassium phosphate pH 6.2. To obtain crystals suitable for X-ray diffraction, the hanging drop vapor-diffusion method was used and the initial crystallization conditions were further optimized by varying the concentration of protein, pH and salts. Crystals, 0.08 × 0.08 × 0.12 mm in dimensions, could be observed within a week.

Data collection and processing

For X-ray diffraction data collection, a single crystal was briefly immersed into reservoir solution containing 20% glycerol, used as a cryoprotectant, and was immediately flash-cooled in a 100 K nitrogen stream. Native X-ray diffraction data were collected using an ADSC Q315r CCD detector on beamline 5C at Pohang Accelerator Laboratory (PAL; Korea) using 1 oscillation and with a crystal-to-detector distance of 150 mm. The crystal was exposed for 1 sec per image. A data set was collected to 1.5 Å resolution from a single crystal. The data were indexed and scaled with the HKL-2000 software package (Otwinowski and Minor, 1997).

Model building and refinement

The structure was solved by molecular replacement using MOLREP and PHASER with diffraction data in the 50–1.5 Å resolution range (McCoy *et al.*, 2007; Vagin and Teplyakov, 2010). We initially used the EcTssL (PDB ID, 3U66) structure as a search model; however, we failed to determine the structure. Instead, a correct solution could be obtained when a C-terminally truncated EcTssL structure, lacking the residues 159–178, was used. The best MR model gave a Z-score

Table 1. Data collection and refinement statistics of VcTssL

Statistics	VcTssL
Data collection	
Space group	$P6_1$
Cell dimensions (Å)	
a, b, c (Å)	78.361 78.361 49.456
α, β, γ (°)	90 90 120
Resolution (Å)	50.00–1.50 (1.53–1.50)[a]
R_{merge}[b] (%)	6.6 (33.9)
I/σ (I)	59 (6.63)
Completeness (%)	99.76 (99.89)
Redundancy	11.0 (8.5)
Structure refinement	
Resolution (Å)	27.98–1.499 (1.54–1.499)
No. of reflections	27803 (2768)
R_{work}[c] / R_{free}[d]	17.74 / 19.09
No. atoms, Proteins/ Water/Ligand	1307 / 67 / 6
R.m.s.deviation	
bond lengths (Å)	0.006
angles (°)	1.10
Average B-factor (Å^2)	23.40
Ramachandran plot (%)	
favored region	97.4
Outliers	0.65
PDB accession code	4V3I

[a] The numbers in parentheses are statistics from the highest resolution shell.
[b] $R_{merge} = \Sigma |I_{obs} - I_{avg}| / I_{obs}$, where I_{obs} is the observed intensity of individual reflection and I_{avg} is average over symmetry equivalents.
[c] $R_{work} = \Sigma ||F_o| - |F_c|| / \Sigma |F_o|$, where $|F_o|$ and $|F_c|$ are the observed and calculated structure factor amplitudes, respectively.
[d] R_{free} was calculated with 5% of the data.

of RFZ=4.0 and TFZ=3.7, a log-likelihood gain of 32.7, and an R_{free} of 47.8% in the 30–1.5 Å resolution range. With a correctly positioned model, Fo–Fc and 2 Fo–Fc maps were calculated, and model building was performed using the program Coot (Emsley and Cowtan, 2004). The model was further refined using CCP4 refmac5 and CNS (Brunger *et al.*, 1998; Murshudov *et al.*, 2011). The data processing statistics are summarized in Table 1.

Results and Discussion

Overall structure of *V. cholerae* TssL

To investigate the functional mechanism of the core components of the type VI secretion system, we determined the crystal structure of TssL from *Vibrio cholerae* at 1.5 Å resolution. The predicted C-terminal transmembrane helix (38 residues) was excluded for the purpose of crystallization. In addition to this truncation, limited proteolysis at a 10^{-4} ratio of trypsin, was carried out at 4°C prior to crystallization to facilitate protein packing. The cytoplasmic domain structure of VcTssL (*V. cholerae* TssL, VCA0115, residues 1–219) was determined at 1.5 Å resolution by molecular replacement (MR). To get the MR solution, we used the C-terminal loop (residues 159–178) truncated *E. coli* TssL (PDB ID, 3U66) as a model. One VcTssL molecule was found in an asymmetric unit with the crystallographic $P6_1$ symmetry, consistent with the size-exclusion chromatography data (data not shown).

The topology of VcTssL represents nine α-helices that can be separated into N- and C-terminal α-helical bundles (Fig. 1A). The N-terminal bundle consists of three α-helices (α1 to α3) with the length of ~ 30 Å. α1 helix is bent about 40°, probably due to crystal packing. Thirty-three residues on the N-terminal end and 4 residues on loop α1-α2 are not visible because of their flexibility. The C-terminal bundle consists of four helices (α5 to α7) including one turn helix αB, which is not shown in other orthologous structures (see below). All the helices in this bundle are shorter by about 1–2 turns compared to those in the N-terminal bundle. The two N- and C-terminal bundles are linked by 26 residues that contain two 1-turn α-helices (αA and α4). Although the linker helices protrude from the helical bundles and are vicinal to the N-terminal bundle, they do not contribute to the association of the two bundles (Fig. 1B). Instead, the N-terminal α3 helix and the C-terminal α6 helix mediate packing of the two helical bundles by extensive hydrophobic interactions (Fig. 1C).

Interestingly, a peptide fragment composed of 5 amino acids is bound at the cleft between the N- and C-terminal helical bundles (Fig. 1A). After model building, the sequence of the five amino acids was deduced to be Asp-Leu-Thr-Arg-Pro, which corresponds to residues199 to 203. This 5-residue fragment is named the C-terminal tail and is described in detail in the following sections.

Comparison with TssL homologs

Recent reports have shown two crystal structures of the cytoplasmic domain of TssL from *E. coli* (EcTssL) and *F. novicida* (FnTssL) (Durand *et al.*, 2012; Robb *et al.*, 2012). Inspite of the low sequence identity, all three structures share similar overall folds of α-helical bundles (Fig. 2). Sequence identity of VcTssL compared to EcTssL and FnTssL is less than 20% and suggests that the function of TssL could be largely dependent on specific structural units (Fig. 2A). Since the root-mean-square deviation (RMSD) of VcTssL is closer to that of EcTssL (1.59 Å, 134 C_α) than FnTssL (1.90 Å, 130 C_α), the crystal structure of VcTssL is more similar to EcTssL than FnTssL (Fig. 2B–D).

Two major differences are found when the three structures are compared. Firstly, the number of helices differs, i.e., VcTssL, EcTssL, and FnTssL have 9, 8, and 7 helices, respectively. VcTssL has additional helices (αA and αB) in each of the linker region and C-terminal bundle, whereas EcTssL

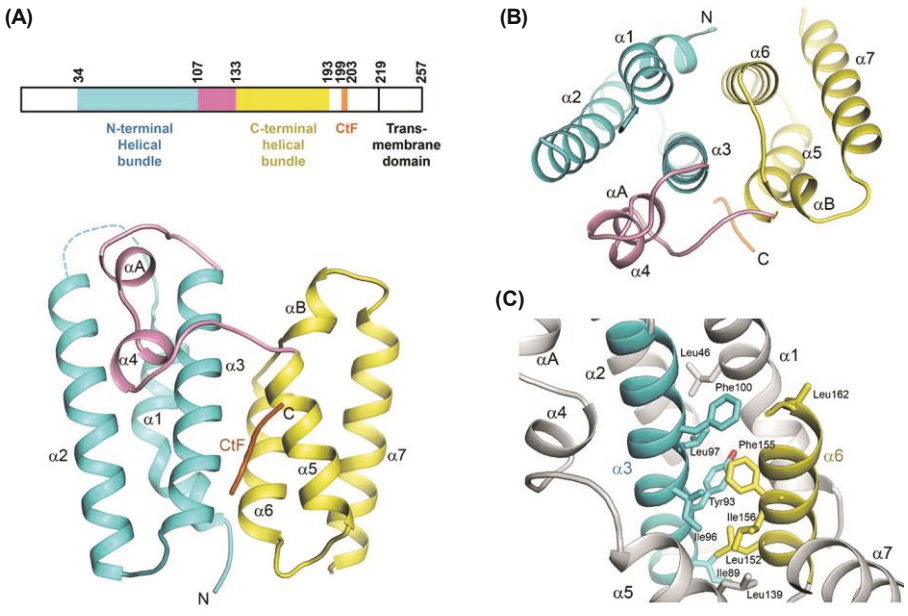

Fig. 1. Crystal structure of VcTssL. (A) The upper panel represents the schematic diagram of domain organization of VcTssL. The colored region indicates the structure-determined region as shown in the lower panel. The overall structure of VcTssL is shown in ribbon representation in which the N- and C-terminal helical bundles are shown in cyan and yellow, respectively. The linker region containing two short α helices and the C-terminal fragment are colored in pink and orange, respectively. (B) The top view of VcTssL structure is shown by a 120° rotation along the X-axis from the orientation of the Fig. 1A. (C) Hydrophobic interactions between the helix α3 and α6 by colored in cyan and yellow, respectively. Other helices are shown in grey for clarifying.

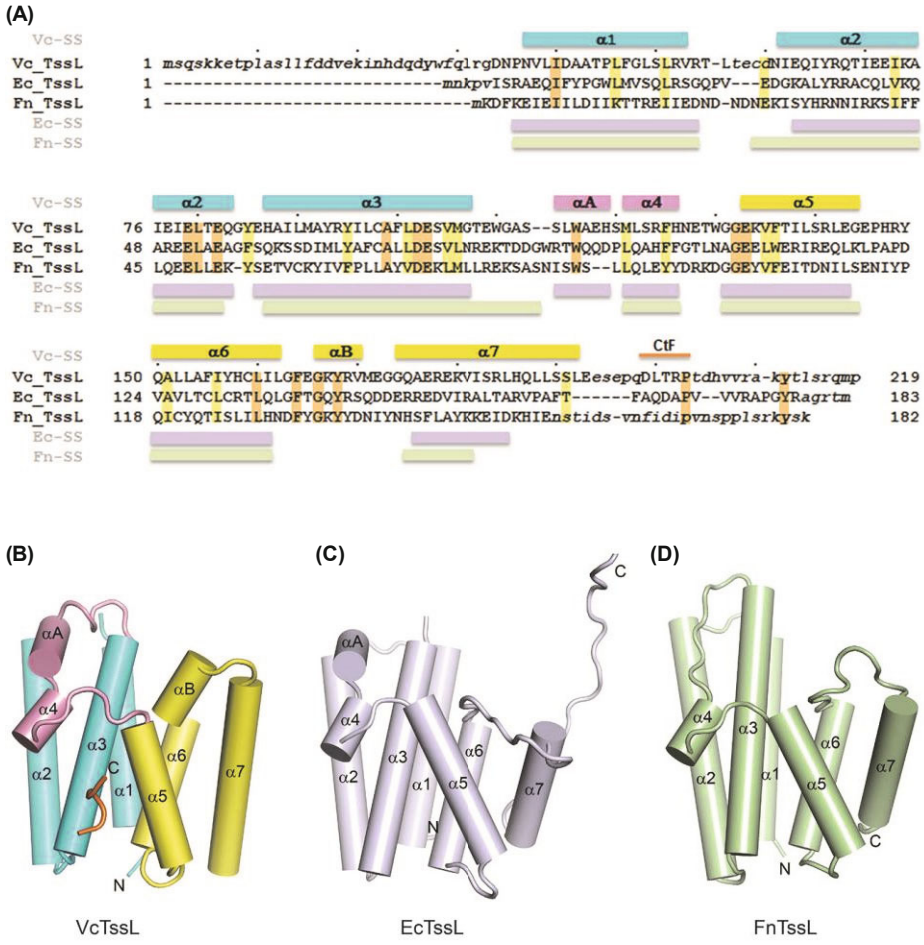

Fig. 2. Comparison of the structures of TssL homologous. (A) Structure-based sequence alignment of *V. cholerae* TssL, VcTssL; *E. coli* TssL, EcTssL, and *F. novicida* TssL, FnTssL. The secondary structure elements of VcTssL (Vc-SS) are shown above the alignment using the same colors as Fig. 1A. The secondary structure elements of EcTssL (Ec-SS) and FnTssL (Fn-SS) are shown below the alignment in light blue and light green, respectively. Depending on their similarity, conserved residues are shown either in orange or yellow. Residues that are disordered in the structures are shown in lowercase and italics. CtF indicates C-terminal fragment. (B) Schematic representation of the VcTssL structure in the same color as the Vc-SS. (C) The structure of EcTssL, in the same orientation as VcTssL, is shown in light blue. (D) The structure of FnTssL, in the same orientation as the two other structures, is shown in light green.

has an additional helix only in the linker region, and no additional helices are found in FnTssL. In contrast to VcTssL and EcTssL, α3 helix in FnTssL is rather extended owing to one additional turn. The linker region is shortened leaving no space for an additional helix. The varied conformations of the α6-α7 loops indicate that the αB in VcTssL could be generated depending on sequence information (Fig. 2B–D). The second major difference is that the conformation of C-termini in the three different structures is different. As mentioned above, the fragmented C-terminal tail in cytoplasmic VcTssL is bound in the cleft of the two helical bundles (Fig. 2B). The C-terminus of EcTssL displays a very long loop (20 amino acids) due to crystal packing, while that in FnTssL is mostly disordered (Fig. 2C–D). Additionally, EcTssL is dimeric in the crystal packing but both VcTssL and FnTssL are monomeric either in solution or in the asymmetric unit. These features represent the intrinsic flexibility of the C-terminal loops following the helix α7. Additionally, both terminal ends of VcTssL and EcTssL point towards the same direction indicating the location of C-terminal transmembrane domain.

Unique feature of *V. cholerae* TssL

As mentioned previously, in VcTssL a C-terminal fragment containing five residues binds to the central cleft clearly (Fig. 3A). This fragment interacts with the four α-helices (α3–α6) via hydrogen bonding or hydrophobic interactions, the α3 helix contributes mainly to capture it (Fig. 3B). The side chains of Asp199 and Thr201 interact with the main chain of Asp88 and the side chain of His126 by water mediated hydrogen bonds, respectively. Similarly, the main chain of Pro203 interacts with the side chain of Thr137 by water mediated hydrogen bonding. The carbonyl oxygen of Arg202 has a direct hydrogen bond with the side chain of Arg141. Leu200 is stabilized by hydrophobic interactions with Ile89, Ile138, Leu142, Leu152, and Tyr149. Thus, the C-terminal fragment tightly associates with the helical bundles.

Based on the bioinformatic analysis, TssL contains a single transmembrane region at the C-terminal end (Aschtgen *et al.*, 2012). Currently, there is no structure available for full length TssL. The long C-terminal tail shown in the crystal structure of EcTssL could provide the possible location of the transmembrane domain. However, it was found to be an artifact of crystal packing. Furthermore, there is discrepancy concerning the location of the C-terminus between the structures of VcTssL and EcTssL. In VcTssL, the C-terminal fragment sits on the central cleft between the two helical bundles (Fig. 1A) and is a very interesting feature unique to this structure. How the C-terminal fragment can be shown in the structure needs to be investigated.

To assess if the fragment is an intra-molecular or an inter-

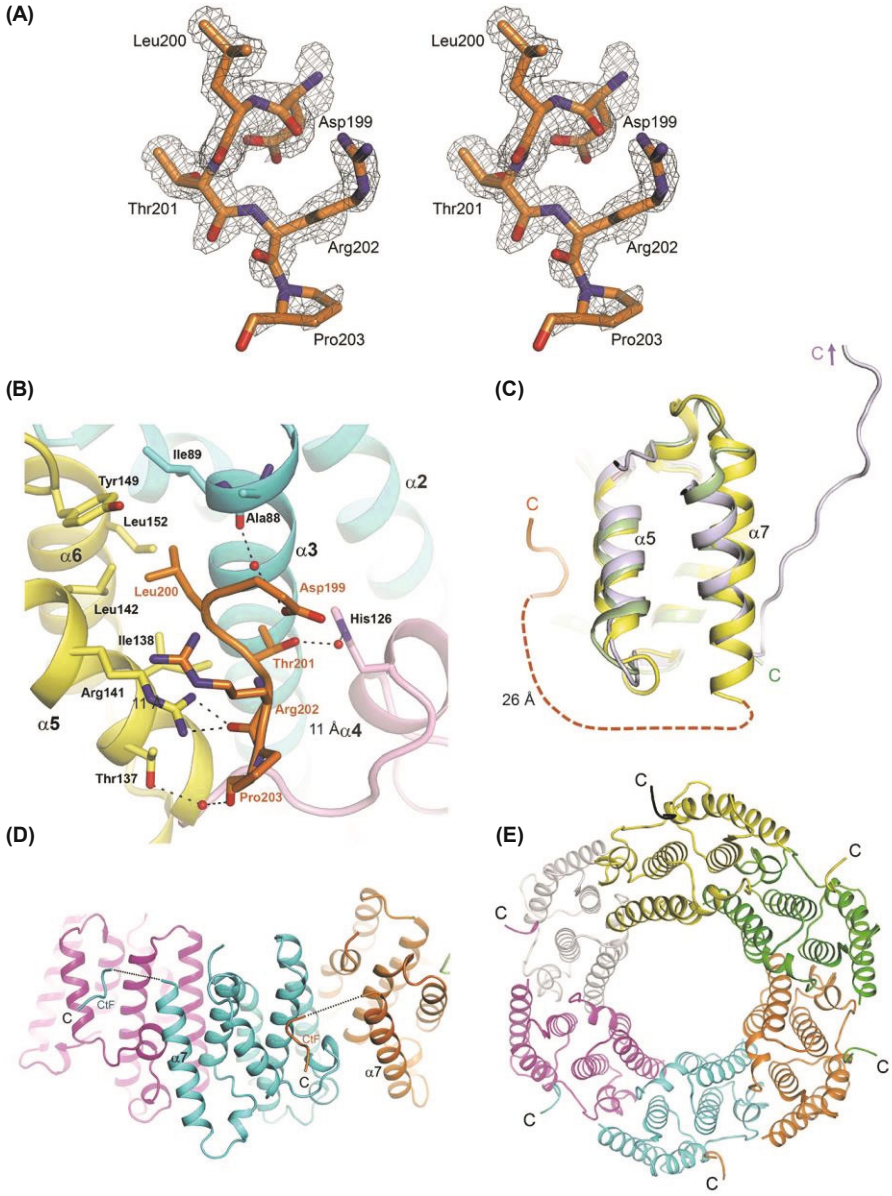

Fig. 3. Unique features of VcTssL. (A) Stereo view of the 2Fo–Fc electron density at 1.5 Å resolution for the C-terminal fragment (CtF), contoured at 1.0σ. (B) Interactions between the C-terminal fragment and helical bundles. The C-terminal fragment is shown in orange. Oxygen and nitrogen atoms are shown in red and blue, respectively. Small spheres indicate water molecules. Dotted lines indicate intermolecular hydrogen bonds between the C-terminal fragment and helical bundles. (C) Overlay of the C-terminal helices α5 and α7 of VcTssL (yellow), EcTssL (light blue), and FnTssL (light green). The C-terminal fragment and end of helix α7 are connected by a dotted line. The three different C-termini of the TssL structures are marked. 26 Å distance was measured directly from the end of α7 to the start of the C-terminal fragment. (D) Schematic drawing of three crystallographic symmetry related molecules of VcTssL are shown in magenta, cyan and orange. The C-terminal fragments and the end of α7 helix of the next symmetry related molecule are linked by black dotted lines with labels of 11 Å distance. (E) Schematic drawing of the symmetry operations of VcTssL in six different colors. Each C-termini within the C-terminal fragments is marked with 'C'. The helical bundles and C-terminal fragment belong to the black colored C-terminal fragment and grey colored helical bundles are not shown.

molecular part, we initially measured the distance from the helix α7 end to the N-terminal end of the fragment (Fig. 3C). If this fragment is assumed to be intra-molecular, there is still a five residue-size gap between each end. However, the distance is ~26 Å, which corresponds to the fully extended peptide length of eight amino acids. Based on this, the fragment cannot be envisaged to be intra-molecular. Next, we measured the distance from the N-terminal fragment to the helix α7 in a symmetry related molecule (Fig. 3D). This distance was ~11 Å that is affords linking between the five missing residues Therefore, the C-terminal fragment may be appeared by crystallographic packing as similar to that of EcTssL (Fig. 3E). Another possibility that might explain this arises from the limited proteolysis of VcTssL just before crystallization. After trypsin digestion, we confirmed the position of the cleavage protein somewhere within the C-terminal region, and the resulting protein migrated about 6 kDa lower on SDS-PAGE (data not shown). Hence, it might be possible that the fragment originating due to trypsin digestion binds to the central cleft as an oligopeptide. However, Arg or Lys is not present in the five missing residues connecting the helix α7 and the bound fragment. Taken together, we conclude that the bound C-terminal fragment is not the product of intramolecular but of intermolecular association due to crystallographic packing effect. This incidental feature of VcTssL may provide insights into molecular partner screening for the cytoplasmic domain of TssL. In addition, it may help design molecular probes or chemicals for functional studies of TssL.

Acknowledgements

This research was supported by Kyungpook National University Research Fund 2013 to JHC.

References

Aschtgen, M.S., Thomas, M.S., and Cascales, E. 2010. Anchoring the type VI secretion system to the peptidoglycan: TssL, TagL, TagP... what else? *Virulence* **1**, 535–540.

Aschtgen, M.S., Zoued, A., Lloubes, R., Journet, L., and Cascales, E. 2012. The C-tail anchored TssL subunit, an essential protein of the enteroaggregative *Escherichia coli* Sci-1 Type VI secretion system, is inserted by YidC. *Microbiologyopen* **1**, 71–82.

Bingle, L.E., Bailey, C.M., and Pallen, M.J. 2008. Type VI secretion: a beginner's guide. *Curr. Opin. Microbiol.* **11**, 3–8.

Brunger, A.T., Adams, P.D., Clore, G.M., DeLano, W.L., Gros, P., Grosse-Kunstleve, R.W., Jiang, J.S., Kuszewski, J., Nilges, M., Pannu, N.S., *et al.* 1998. Crystallography & NMR system: A new software suite for macromolecular structure determination. *Acta Crystallogr. D Biol. Crystallogr.* **54**, 905–921.

Cascales, E. 2008. The type VI secretion toolkit. *EMBO Rep.* **9**, 735–741.

Cascales, E. and Cambillau, C. 2012. Structural biology of type VI secretion systems. *Philos. Trans R Soc. Lond B Biol. Sci.* **367**, 1102–1111.

Durand, E., Zoued, A., Spinelli, S., Watson, P.J., Aschtgen, M.S., Journet, L., Cambillau, C., and Cascales, E. 2012. Structural characterization and oligomerization of the TssL protein, a component shared by bacterial type VI and type IVb secretion systems. *J. Biol. Chem.* **287**, 14157–14168.

Economou, A., Christie, P.J., Fernandez, R.C., Palmer, T., Plano, G.V., and Pugsley, A.P. 2006. Secretion by numbers: Protein traffic in prokaryotes. *Mol. Microbiol.* **62**, 308–319.

Emsley, P. and Cowtan, K. 2004. Coot: model-building tools for molecular graphics. *Acta. Crystallogr. D Biol. Crystallogr.* **60**, 2126–2132.

Faruque, S.M., Albert, M.J., and Mekalanos, J.J. 1998. Epidemiology, genetics, and ecology of toxigenic *Vibrio cholerae*. *Microbiol. Mol. Biol. Rev.* **62**, 1301–1314.

Felisberto-Rodrigues, C., Durand, E., Aschtgen, M.S., Blangy, S., Ortiz-Lombardia, M., Douzi, B., Cambillau, C., and Cascales, E. 2011. Towards a structural comprehension of bacterial type VI secretion systems: characterization of the TssJ-TssM complex of an *Escherichia coli* pathovar. *PLoS Pathog.* **7**, e1002386.

Filloux, A. 2009. The type VI secretion system: a tubular story. *EMBO J.* **28**, 309–310.

Jani, A.J. and Cotter, P.A. 2010. Type VI secretion: not just for pathogenesis anymore. *Cell Host Microbe* **8**, 2–6.

Ma, A.T. and Mekalanos, J.J. 2010. *In vivo* actin cross-linking induced by *Vibrio cholerae* type VI secretion system is associated with intestinal inflammation. *Proc. Natl. Acad. Sci. USA* **107**, 4365–4370.

MacIntyre, D.L., Miyata, S.T., Kitaoka, M., and Pukatzki, S. 2010. The *Vibrio cholerae* type VI secretion system displays antimicrobial properties. *Proc. Natl. Acad. Sci. USA* **107**, 19520–19524.

McCoy, A.J., Grosse-Kunstleve, R.W., Adams, P.D., Winn, M.D., Storoni, L.C., and Read, R.J. 2007. Phaser crystallographic software. *J. Appl. Cryst.* **40**, 658–674.

Miyata, S.T., Kitaoka, M., Wieteska, L., Frech, C., Chen, N., and Pukatzki, S. 2010. The *Vibrio cholerae* Type VI secretion system: Evaluating its role in the human disease cholera. *Front. Microbiol.* **1**, 117.

Murshudov, G.N., Skubak, P., Lebedev, A.A., Pannu, N.S., Steiner, R.A., Nicholls, R.A., Winn, M.D., Long, F., and Vagin, A.A. 2011. REFMAC5 for the refinement of macromolecular crystal structures. *Acta Crystallogr. D Biol. Crystallogr.* **67**, 355–367.

Otwinowski, Z. and Minor, W. 1997. Processing of X-ray diffraction data collected in oscillation mode. *Method Enzymol.* **276**, 307–326.

Pukatzki, S., Ma, A.T., Sturtevant, D., Krastins, B., Sarracino, D., Nelson, W.C., Heidelberg, J.F., and Mekalanos, J.J. 2006. Identification of a conserved bacterial protein secretion system in *Vibrio cholerae* using the dictyostelium host model system. *Proc. Natl. Acad. Sci. USA* **103**, 1528–1533.

Pukatzki, S., McAuley, S.B., and Miyata, S.T. 2009. The type VI secretion system: translocation of effectors and effector-domains. *Curr. Opin. Microbiol.* **12**, 11–17.

Robb, C.S., Nano, F.E., and Boraston, A.B. 2012. The structure of the conserved type six secretion protein TssL (DotU) from *Francisella novicida*. *J. Mol. Biol.* **419**, 277–283.

Russell, A.B., Hood, R.D., Bui, N.K., LeRoux, M., Vollmer, W., and Mougous, J.D. 2011. Type VI secretion delivers bacteriolytic effectors to target cells. *Nature* **475**, 343–347.

Russell, A.B., Peterson, S.B., and Mougous, J.D. 2014. Type VI secretion system effectors: poisons with a purpose. *Nat. Rev. Microbiol.* **12**, 137–148.

Schwarz, S., Hood, R.D., and Mougous, J.D. 2010. What is type VI secretion doing in all those bugs? *Trends Microbiol.* **18**, 531–537.

Silverman, J.M., Brunet, Y.R., Cascales, E., and Mougous, J.D. 2012. Structure and regulation of the type VI secretion system. *Annu. Rev. Microbiol.* **66**, 453–472.

Vagin, A. and Teplyakov, A. 2010. Molecular replacement with MOLREP. *Acta Crystallogr. D Biol. Crystallogr.* **66**, 22–25.

Zheng, J., Shin, O.S., Cameron, D.E., and Mekalanos, J.J. 2010. Quorum sensing and a global regulator TsrA control expression of type VI secretion and virulence in *Vibrio cholerae*. *Proc. Natl. Acad. Sci. USA* **107**, 21128–21133.

Zoued, A., Brunet, Y.R., Durand, E., Aschtgen, M.S., Logger, L., Douzi, B., Journet, L., Cambillau, C., and Cascales, E. 2014. Architecture and assembly of the Type VI secretion system. *Biochim. Biophys. Acta* **1843**, 1664–1673.